

Transmit Beamforming Design for ISAC with Stacked Intelligent Metasurfaces

Shunyu Li, *Student Member, IEEE*, Fan Zhang, *Student Member, IEEE*, Tianqi Mao, *Member, IEEE*, Rui Na, Zhaocheng Wang, *Fellow, IEEE*, and George K. Karagiannidis, *Fellow, IEEE*

Abstract—This paper proposes a transmit beamforming strategy for the integrated sensing and communication (ISAC) systems enabled by the novel stacked intelligent metasurface (SIM) architecture, where the base station (BS) simultaneously performs downlink communication and radar target detection via different beams. To ensure superior dual-function performance simultaneously, we design the multi-layer cascading beamformer by maximizing the sum rate of the users while optimally shaping the normalized beam pattern for detection. A dual-normalized differential gradient descent (D^3) algorithm is further proposed to solve the resulting non-convex multi-objective problem (MOP), where gradient differences and dual normalization are employed to ensure a fair trade-off between communication and sensing objectives. Numerical results demonstrate the superiority of the proposed beamforming design in terms of balancing communication and sensing performance.

Index Terms—Stacked intelligent metasurfaces (SIM), reconfigurable intelligent surface (RIS), integrated sensing and communication (ISAC), beamforming.

I. INTRODUCTION

Integrated Sensing and Communication (ISAC) is considered one of the most promising technologies for next-generation wireless networks [1], [2]. Such philosophy aims at realizing the convergence of communication and sensing systems by sharing hardware platforms, spectrum resources, and even waveforms, which can alleviate spectrum congestion and hardware costs [3]. Therefore, this integrated implementation can support many emerging applications such as augmented reality, autonomous driving, and the Industrial Internet of Everything (IoE), where communication and sensing devices with compact deployment are highly demanded [4]–[6].

To further enhance the communication and sensing capabilities, the ISAC framework tends to incorporate the multi-antenna technology for additional spatial degrees of freedom (DoF) achieved by large-scale antenna array [7]. Despite the fascinating capabilities of digital/hybrid beamforming, classical array-based ISAC systems inevitably suffer from excessive power consumption and hardware cost, resulting from the numerous radio frequency (RF) chains or complex feeding

networks with phase shifters and microstrip lines [8], [9]. To solve this problem, the programmable metasurface, also known as reconfigurable intelligent surface (RIS), can be implemented at the transceiver by replacing the classical phased array antenna, where the RF chains and feeding networks are no longer required [10]. In [11], a reconfigurable distributed antenna and reflecting surface aided ISAC system was proposed, combining the distributed gain of the distributed antenna system with the passive beamforming gain of RIS to significantly improve system performance while reducing hardware cost. Besides, [12] developed a RIS-enabled integrated sensing, communication, and computing system where RF chain-free transmissions were realized by using RIS as passive information carriers and modulators.

The aforementioned literature mainly focused on the single-layer metasurface structure, whose ability to control electromagnetic waves may be limited. To this end, the stacked intelligent metasurface (SIM) has recently been proposed as a promising approach which cascades multiple layers of transmissive metasurfaces. This SIM technology can further enhance the degrees of freedom (DoF) in manipulating the electromagnetic environment, which exhibits desirable communication performance in terms of multi-user beamforming [13], [14]. Despite [15] that deployed SIM between the base station and users/targets for ISAC performance enhancement, research on ISAC system design with the transmit SIM architecture is still in its infancy.

In this context, we propose a transmit beamforming design for ISAC systems equipped with SIM at the BS to perform downlink communication and sensing simultaneously. Specifically, we consider dedicated streams for communication and sensing, respectively. To achieve the desired dual-function performance tradeoff, we optimize the reflection coefficients of SIM elements to form the corresponding sensing beam patterns toward the desired target in the 2D angular domain, while maximizing the total communication data rate. Furthermore, we propose the Dual-normalized Differential Gradient Descent (D^3) algorithm to tackle this non-convex multi-objective problem (MOP) with coupled variables induced by the cascaded structure of SIM. The proposed D^3 algorithm uses gradient differences to balance the communication and sensing objectives, while incorporating two levels of normalization. The first normalization equalizes the magnitudes of the communication and sensing gradients, ensuring effective gradient differences, while the second normalization balances the phase shifts between SIM elements for convergence. Simulation results validate the superiority of our proposed transmit beamforming design and elucidate the impact of SIM parameters on dual-function performance, providing useful guidelines for SIM-enabled ISAC implementations.

This work was supported by National Natural Science Foundation of China under Grant No. 62088101. (*Corresponding authors: Tianqi Mao, Rui Na.*)

S. Li, T. Mao and R. Na are with State Key Laboratory of CNS/ATM, Beijing Institute of Technology, Beijing 100081, China. T. Mao is also with Beijing Institute of Technology (Zhuhai), Zhuhai 519088, China. R. Na is also with Yangtze Delta Region Academy of Beijing Institute of Technology (Jiaxing), Jiaxing 314019, China (e-mails: li.shunyu@bit.edu.cn, maotq@bit.edu.cn, narui@bit.edu.cn).

F. Zhang and Z. Wang are with Department of Electronic Engineering, Tsinghua University, Beijing 100084, China (e-mails: zf22@mails.tsinghua.edu.cn, zcwang@tsinghua.edu.cn).

G. K. Karagiannidis is with Department of Electrical and Computer Engineering, Aristotle University of Thessaloniki, Greece and also with Artificial Intelligence & Cyber Systems Research Center, Lebanese American University (LAU), Lebanon (geokarag@auth.gr).

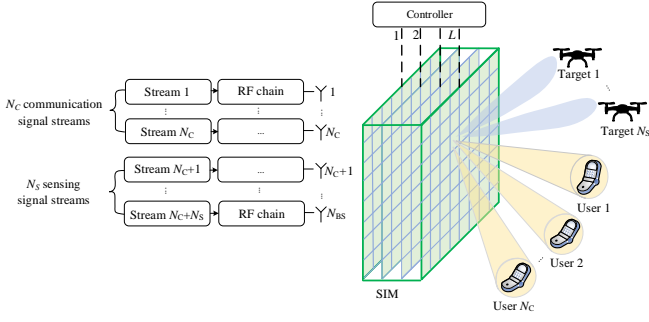


Fig. 1. Illustration of the considered SIM-enabled ISAC system.

II. SYSTEM MODEL FOR SIM-ENABLED ISAC

As shown in Fig. 1, we consider a SIM-enabled ISAC system serving N_C single-antenna users and N_S sensing targets. The transmitter (BS) consists of a SIM planar array illuminated by a uniform linear array (ULA) of N_{BS} antennas. For simplicity and to focus on the SIM-enabled beamforming capabilities, we assume uniform power distribution over the ULA at the base station. Apart from the N_C parallel communication data streams, we assume N_S independent streams for sensing to extend the degrees of freedom (DoF) for the transmit beamforming design, i.e., $N_{BS} \triangleq N_C + N_S$, where the number of communication and sensing signal streams is equal to the number of users and targets, respectively [7], [8].

For clarity, the SIM is assumed to consist of L layers of metasurfaces of size $M = M_r \times M_c$, where M_r and M_c denote the number of meta-atoms in the rows and columns of each metasurface layer, respectively.

According to Rayleigh-Sommerfeld diffraction theory, which is widely employed in SIM-related literature [13]–[17], the inter-layer channel coefficient $w_{m,m'}^l$ from the m' -th meta-atom on the $(l-1)$ -th metasurface layer, i.e., Layer $(l-1)$, to the m -th meta-atom on Layer l , can be expressed by

$$w_{m,m'}^l = \frac{A_t \cos \chi_{m,m'}^l}{r_{m,m'}^l} \left(\frac{1}{2\pi r_{m,m'}^l} - j \frac{1}{\lambda} \right) e^{j2\pi \frac{r_{m,m'}^l}{\lambda}}, \quad (1)$$

where λ is the wavelength, A_t represents the size of each meta-atom, $r_{m,m'}^l$ denotes the transmission distance, while $\chi_{m,m'}^l$ specifies the angle between the propagation direction and the normal direction of the Layer $(l-1)$. By applying (1) to each meta-atom, we obtain the inter-layer diffraction matrix, denoted as $\mathbf{W}^l \in \mathbb{C}^{M \times M}$ for $l = 2, 3, \dots, L$. Besides, we have $\mathbf{W}^1 \in \mathbb{C}^{M \times N_{BS}}$ for $l = 1$, which represents the diffraction matrix from the feeding antenna array to the Layer 1 of the SIM. Additionally, the diagonal phase shift matrix Φ^l of the Layer l of the SIM can be formulated as

$$\Phi^l = \text{diag} \left(e^{j\theta_1^l}, e^{j\theta_2^l}, \dots, e^{j\theta_m^l}, \dots, e^{j\theta_M^l} \right), \quad (2)$$

where $e^{j\theta_m^l}$ denotes the phase shift applied by the m -th meta-atom on Layer l with $\theta_m^l \in [0, 2\pi)$, for $l = 1, 2, \dots, L$ and $m = 1, 2, \dots, M$. Afterwards, the SIM-enabled beamforming matrix $\mathbf{F}_{SIM} \in \mathbb{C}^{M \times N_{BS}}$ can be expressed as

$$\mathbf{F}_{SIM} = \Phi^L \mathbf{W}^L \Phi^{L-1} \mathbf{W}^{L-1} \dots \Phi^1 \mathbf{W}^1. \quad (3)$$

By adopting the Saleh-Valenzuela channel model for MIMO

systems [8], the channel between the SIM and the n -th communication user, i.e., user n , for $n = 1, 2, \dots, N_C$ can be characterized as

$$\mathbf{h}_n = \sqrt{\frac{M}{Q_n}} \sum_{q=1}^{Q_n} g_q^{(n)} \boldsymbol{\alpha}^H \left(\theta_q^{(n)}, \varphi_q^{(n)} \right), \quad (4)$$

where Q_n is the number of resolvable channel paths, while $g_q^{(n)}$ represents the channel gain for $q = 1, 2, \dots, Q_n$. Specifically, for the LOS path, the channel gain is distributed as $g_{q=1}^{(n)} \sim \mathcal{CN}(0, \beta)$, while for NLOS paths, the channel gain is distributed as $g_{q>1}^{(n)} \sim \mathcal{CN}(0, 0.01\beta)$, for $n = 1, \dots, N_C$. Here, β denotes the distance-dependent path loss modeled as $\beta = C_0 d_n^{-\alpha}$, where C_0 is the free space path loss, α is the path loss exponent, and d_n is the distance from the SIM to the user n . Moreover, $\theta_q^{(n)}$ and $\varphi_q^{(n)}$ represent the elevation and azimuth angles of departure (AoD) of the q -th channel path relative to those of the LoS path component. $\boldsymbol{\alpha}(\theta, \varphi) \in \mathbb{C}^{M \times 1}$ denotes the channel steering vector, which is a function of elevation and azimuth angles expressed by

$$\boldsymbol{\alpha}(\theta, \varphi) = \left[1, \dots, e^{-j2\pi(M_r-1)\sin(\theta)\cos(\varphi)\frac{d_x}{\lambda}} \right] \otimes \left[1, \dots, e^{-j2\pi(M_c-1)\sin(\theta)\sin(\varphi)\frac{d_y}{\lambda}} \right], \quad (5)$$

where \otimes stands for the Kronecker product, and d_x and d_y represent the horizontal and perpendicular spacings between adjacent meta-atoms, respectively [18].

The transmit signal at the BS before passing through the SIM is denoted as $\mathbf{x} \in \mathbb{C}^{N_{BS}}$, where $\mathbb{E}\{\mathbf{x}\} = \mathbf{0}$ and $\mathbb{E}\{\mathbf{x}\mathbf{x}^H\} = \mathbf{I}_{N_{BS}}$. The first N_C elements of \mathbf{x} , i.e., x_1, x_2, \dots, x_{N_C} , represent the information symbols for the N_C communication users, while the remaining N_S elements, i.e., $x_{N_C+1}, \dots, x_{N_{BS}}$, correspond to the sensing waveforms for the N_S sensing targets. Hence, the received signals by different users, denoted as $\mathbf{y} \in \mathbb{C}^{N_C \times 1}$, can be expressed as

$$\mathbf{y} = \mathbf{H}\mathbf{F}_{SIM}\mathbf{x} + \mathbf{n}, \quad (6)$$

where $\mathbf{H} \triangleq [\mathbf{h}_1, \mathbf{h}_2, \dots, \mathbf{h}_{N_C}]^T \in \mathbb{C}^{N_C \times M}$ denotes the total channel matrix, and $\mathbf{n} \in \mathbb{C}^{N_C \times 1}$ is the additive white Gaussian noise (AWGN) vector with $\mathbf{n} \sim \mathcal{CN}(\mathbf{0}, \sigma^2 \mathbf{I}_{N_C})$. Here, σ^2 is the noise power at the receivers, and \mathbf{I}_{N_C} is the N_C -by- N_C identity matrix. For user n , both the signals from the other users and sensing targets are regarded as interference. Therefore, the signal-to-interference-plus-noise ratio (SINR) of user n can be expressed as

$$\gamma_n = \frac{\left| [\mathbf{H}\mathbf{F}_{SIM}]_{n,n} \right|^2}{\sum_{i=1, i \neq n}^{N_{BS}} \left| [\mathbf{H}\mathbf{F}_{SIM}]_{n,i} \right|^2 + \sigma^2}, \quad (7)$$

where $[\mathbf{H}\mathbf{F}_{SIM}]_{n,i}$ denotes the element in the n -th row and i -th column of the $\mathbf{H}\mathbf{F}_{SIM}$. Then, the sum rate of the N_C users, according to the Shannon-Hartley theorem, can be written as

$$R_{\text{sum}} = \sum_{n=1}^{N_C} \log_2(1 + \gamma_n). \quad (8)$$

In terms of sensing, communication signals are regarded as supplementary to enhance the sensing signals. Let $\{\psi_1, \psi_2, \dots, \psi_{N_D}\}$ and $\{\phi_1, \phi_2, \dots, \phi_{N_D}\}$ denote the sampling points evenly distributed in the elevation and azimuth angle domains, respectively. Then the beam pattern gain $\mathbf{P}_S \in \mathbb{R}^{N_D \times N_D}$ of the SIM in the direction $\{\psi_j, \phi_k\}$ for $j, k = 1, 2, \dots, N_D$ can be expressed as

$$[\mathbf{P}_S]_{j,k} = \boldsymbol{\alpha}^H(\psi_j, \phi_k) \mathbf{F}_{\text{SIM}} \mathbf{F}_{\text{SIM}}^H \boldsymbol{\alpha}(\psi_j, \phi_k), \quad (9)$$

where $\boldsymbol{\alpha}(\psi_j, \phi_k)$ is the channel steering vector obtained by (5). Then the normalized beam pattern $\bar{\mathbf{P}}_S$ is calculated as

$$\bar{\mathbf{P}}_S = \frac{\mathbf{P}_S}{\|\mathbf{P}_S\|_1}. \quad (10)$$

Given the desired beam pattern $\mathbf{P}_D \in \mathbb{R}^{N_D \times N_D}$, we define the mean square error (MSE) between \mathbf{P}_D and $\bar{\mathbf{P}}_S$ as the beam-matching error [7], [8], calculated as

$$J_{\text{MSE}} = \|\bar{\mathbf{P}}_S - \mathbf{P}_D\|_2^2. \quad (11)$$

Here, $\|\cdot\|_1$ and $\|\cdot\|_2$ denote the ℓ_1 and ℓ_2 norms, respectively.

III. SIM-BASED TRANSMIT BEAMFORMING DESIGN

A. Problem Formulation

In order to facilitate downlink communication and sensing with desirable performance trade-off, an MOP is formulated to maximize the sum rate of users and concurrently minimize the beam-matching error under uniform transmit power allocation. These can be realized by properly configuring the phase shifts imposed by each meta-atom in the SIM. Denoting $\boldsymbol{\vartheta} \triangleq \{\theta^1, \theta^2, \dots, \theta^L\}$ as the set of optimization variables with $\boldsymbol{\theta}^l \triangleq [\theta_1^l, \theta_2^l, \dots, \theta_M^l]^T$, the MOP is shown as

$$\text{P1: } \max_{\boldsymbol{\vartheta}} R_{\text{sum}} \quad (12a)$$

$$\min_{\boldsymbol{\vartheta}} J_{\text{MSE}} \quad (12b)$$

$$\text{s.t. } \theta_m^l \in [0, 2\pi), \quad (12c)$$

$$\forall l = 1, 2, \dots, L,$$

$$\forall m = 1, 2, \dots, M.$$

Following [19], we apply the weighted-sum method to problem (P1), transforming the MOP into a single objective problem (SOP) written as

$$\text{P2: } \min_{\boldsymbol{\vartheta}} J_{\text{MSE}} - R_{\text{sum}} \quad (13a)$$

$$\text{s.t. } \theta_m^l \in [0, 2\pi), \quad (13b)$$

$$\forall l = 1, 2, \dots, L,$$

$$\forall m = 1, 2, \dots, M.$$

The problem (P2) is inherently non-convex due to the form of the objective function in (13a). Furthermore, the strong coupling among the multiple phase shift matrices across the L layers of the SIM makes the problem even more intractable.

B. D^3 Algorithm

To address the aforementioned problem, we propose an efficient Dual-Normalized Differential Gradient Descent (D^3)

algorithm to achieve a quasi-optimal solution. More specifically, our approach addresses a MOP that includes both communication and sensing tasks. It includes gradient differences and additional normalization steps that adjust the gradient components to similar scales across different tasks. This dual-normalization ensures that the optimization process achieves a balanced trade-off between communication and sensing tasks, and avoids over-promoting any single objective.

First, the phase shifts $\theta_m^l \in [0, 2\pi)$ for $l = 1, 2, \dots, L$ and $m = 1, 2, \dots, M$ are initialized as, e.g., a uniform random distribution. Next, the partial derivatives of J_{MSE} in (13a) with respect to θ_m^l are derived as

$$\frac{\partial J_{\text{MSE}}}{\partial \theta_m^l} = \frac{1}{N_D^2} \sum_{j=1}^{N_D} \sum_{k=1}^{N_D} 2 \left([\bar{\mathbf{P}}_S]_{j,k} - [\mathbf{P}_D]_{j,k} \right) \cdot [\bar{\mathbf{E}}]_{j,k}, \quad (14)$$

where $\bar{\mathbf{E}}$ represents the partial derivatives of $\bar{\mathbf{P}}_S$ in terms of phase shifts θ_m^l , expressed as

$$[\bar{\mathbf{E}}]_{j,k} = \frac{\|\mathbf{P}_S\|_1 [\mathbf{E}]_{j,k} - [\mathbf{P}_S]_{j,k} \|\mathbf{E}\|_1}{\|\mathbf{P}_S\|_1^2}. \quad (15)$$

Furthermore, \mathbf{E} denotes the partial derivatives of \mathbf{P}_S with respect to phase shifts θ_m^l , which can be calculated as

$$[\mathbf{E}]_{j,k} = 2 \text{Im} \{ e^{j\theta_m^l} \boldsymbol{\alpha}(\psi_j, \phi_k)^H \mathbf{V}_{:,m}^l \mathbf{U}_{m,:}^l \mathbf{F}_{\text{SIM}}^H \boldsymbol{\alpha}(\psi_j, \phi_k) \}. \quad (16)$$

$\text{Im} \{ \cdot \}$ denotes the imaginary part, and $\mathbf{V}_{:,m}^l$ and $\mathbf{U}_{m,:}^l$ denote the m -th column of \mathbf{V}^l and the m -th row of \mathbf{U}^l , respectively, which are defined by

$$\mathbf{U}^l \triangleq \begin{cases} \mathbf{W}^l \boldsymbol{\Phi}^{l-1} \mathbf{W}^{l-1} \dots \boldsymbol{\Phi}^2 \mathbf{W}^2 \boldsymbol{\Phi}^1 \mathbf{W}^1, & \text{if } l \neq 1, \\ \mathbf{W}^1, & \text{if } l = 1, \end{cases} \quad (17)$$

$$\mathbf{V}^l \triangleq \begin{cases} \boldsymbol{\Phi}^L \mathbf{W}^L \boldsymbol{\Phi}^{L-1} \mathbf{W}^{L-1} \dots \boldsymbol{\Phi}^{l+1} \mathbf{W}^{l+1}, & \text{if } l \neq L, \\ \mathbf{I}_M, & \text{if } l = L. \end{cases} \quad (18)$$

Besides, the partial derivatives of R_{sum} in (13a) with respect to θ_m^l are derived as

$$\frac{\partial R_{\text{sum}}}{\partial \theta_m^l} = 2 \log_2 e \sum_{p=1}^{N_C} \delta_p \left(\eta_{p,p} - \gamma_p \sum_{q=1, q \neq p}^{N_C} \eta_{p,q} \right), \quad (19)$$

where δ_p and $\eta_{p,q}$ in (19) are given by [13]

$$\delta_p = \frac{1}{\sum_{q=1}^{N_C} \left| [\mathbf{H}\mathbf{F}_{\text{SIM}}]_{p,q} \right|^2 + \sigma^2}, \quad (20)$$

$$\eta_{p,q} = \text{Im} \left\{ \left[\mathbf{H}\mathbf{V}^l \right]_{p,m} \left[\mathbf{U}^l \right]_{m,q} \left[\mathbf{H}\mathbf{F}_{\text{SIM}} \right]_{p,q}^* e^{j\theta_m^l} \right\}. \quad (21)$$

Inspired by the gradient updating strategy in [20], the partial derivatives obtained from (14) and (19) are then normalized in an element-wise manner. Afterwards, the corresponding differential gradient $\mathbf{G} \in \mathbb{C}^{M \times L}$, can be expressed as

$$[\mathbf{G}]_{m,l} = w_1 \frac{\frac{\partial J_{\text{MSE}}}{\partial \theta_m^l}}{\sqrt{\left(\frac{\partial J_{\text{MSE}}}{\partial \theta_m^l} \right)^2 + \epsilon}} - w_2 \frac{\frac{\partial R_{\text{sum}}}{\partial \theta_m^l}}{\sqrt{\left(\frac{\partial R_{\text{sum}}}{\partial \theta_m^l} \right)^2 + \epsilon}}, \quad (22)$$

TABLE I
SIMULATION PARAMETERS

Parameter	Value
Carrier frequency f_c (GHz)	28
Thickness of the SIM (m)	0.05
Total transmission power (dBm)	20
BS antenna gain (dBi)	5
User antenna gain (dBi)	0
Path loss constant C_0 (dB)	-32
Path loss exponent α	3.5
AWGN noise power σ^2 (dBm)	-104
Distance of user n d_n (m)	[10, 20]
Number of users N_C	4
Number of targets N_S	2
Number of sample points N_D	36
Elevation angle range ($^\circ$)	[-90, 90]
Azimuth angle range ($^\circ$)	[-90, 90]

where w_1 and w_2 denote the weights of the communication and sensing metrics, respectively. ϵ is the smoothing term as a small constant parameter, typically set to 10^{-8} [20].

Additionally, in order to mitigate gradient explosion and vanishing issues during optimization [16], global normalization is applied to the differential gradient. Thus, the dual-normalized differential gradient $\overline{\mathbf{G}}$ can be expressed as

$$[\overline{\mathbf{G}}]_{m,l} = \frac{\pi}{\max(\mathbf{G})} \cdot [\mathbf{G}]_{m,l}, \quad (23)$$

where $m = 1, 2, \dots, M$, $l = 1, 2, \dots, L$, and $\max(\cdot)$ denotes the operation of extracting the largest element.

Ultimately, the phase shifts $\theta_m^l \in \mathcal{D}$ across each meta-atom in SIM can be updated via $\overline{\mathbf{G}}$ at each iteration, expressed as

$$\theta_m^l \leftarrow \theta_m^l - \mu \cdot [\overline{\mathbf{G}}]_{m,l}, \quad (24)$$

where μ is the step size. Specifically, we adopt an exponentially decreasing learning rate schedule as the iteration proceeds, which is updated by [16]

$$\mu \leftarrow \mu\beta, \quad (25)$$

where β is a hyperparameter determining the decay rate, satisfying $0 < \beta < 1$.

By iteratively applying (14)-(25), the objective function (13a) will reach convergence when its decrease is smaller than a preset threshold or reaching the maximum iteration number.

IV. NUMERICAL RESULTS

This section validates the effectiveness of the transmit beamforming design with the proposed D^3 algorithm. The simulation parameters are summarized in Table I. The desired beam pattern for sensing is assumed as

$$[\mathbf{P}_D]_{j,k} = \begin{cases} 1 & \text{if } (j, k) \in \{(9, 27), (27, 9)\}, \\ 0 & \text{otherwise,} \end{cases} \quad (26)$$

where $j, k = 1, 2, \dots, N_D$ correspond to specific elevation and azimuth angles. Specifically, indices 9 and 27 correspond to the angle ranges $[-45^\circ, -40^\circ]$ and $[45^\circ, 50^\circ]$, respectively.

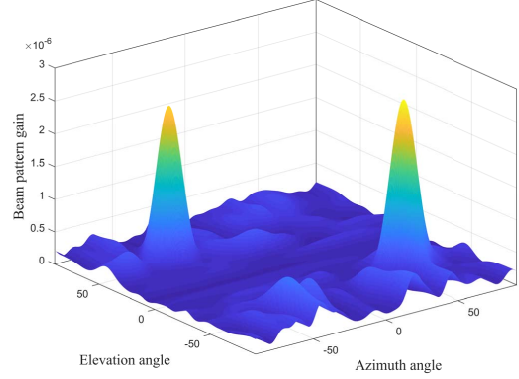


Fig. 2. Transmit beam patterns in the angle space with the proposed beamforming design.

To prevent premature convergence to a local optimum due to inappropriate initialization, we generate five sets of initial phase shifts and run the D^3 algorithm in parallel for each set. The algorithm iterates until either the relative change in the objective function falls below a threshold of 10^{-6} or the maximum number of 60 iterations is reached. Unless otherwise specified, we set the initial learning rate to $\eta = 1$ and the decay parameter to $\beta = 0.5$. After parallel execution, we choose the solution that minimizes $J_{\text{MSE}} - R_{\text{sum}}$ as the quasi-optimal solution for the problems (P1) and (P2) [16].

Figure 2 shows the beam pattern obtained by the proposed beamforming design using the D^3 algorithm, where $M = 100$, $L = 7$, and $w_1 = w_2 = 1$. It can be observed that the beam pattern gain reaches its maximum (about 2.5×10^{-6}) in the directions towards the sensing targets within the regions of $[-45^\circ, -40^\circ]$ in elevation angle space and $[45^\circ, 50^\circ]$ in azimuth angle space, as well as $[45^\circ, 50^\circ]$ in elevation angle space and $[-45^\circ, -40^\circ]$ in azimuth angle space, where the beam-matching error is calculated as $J_{\text{MSE}} = 0.0526$. Meanwhile, the beam peaks for the four communication users are located at $(-60^\circ, -45^\circ)$, and $(-60^\circ, -35^\circ)$. Although the average strength of the communication beams is not comparable to the sensing beams, i.e., below the gain of 0.75×10^{-6} , superior data throughput with $R_{\text{sum}} = 15$ bit/s/Hz can be achieved with the proposed D^3 algorithm. Therefore, the proposed beamforming design successfully realizes a desirable balance between sensing and communication functions.

Figure 3 illustrates the performance comparison of different weighting coefficients w_1 and w_2 with varying numbers of meta-atoms M . The weighting coefficients w_1 and w_2 dictate the trade-off between sensing and communication performance. When $w_1 = 1$ and $w_2 = 0$, the D^3 algorithm functions as a sensing-only scheme, while $w_1 = 0$ and $w_2 = 1$ conversely represents a communication-only scheme. For cases where both w_1 and w_2 are non-zero, the system functions as an ISAC scheme, with their ratio determining the priority of sensing or communication in the system. It can be observed that the sensing-only scheme ($w_1 = 1$, $w_2 = 0$) exhibits poor communication performance, with sum rates that are almost nil. In contrast, the ISAC scheme with $w_1 = w_2 = 1$ achieves a sum rate approaching that of the communication-only scheme ($w_1 = 0$, $w_2 = 1$), while still

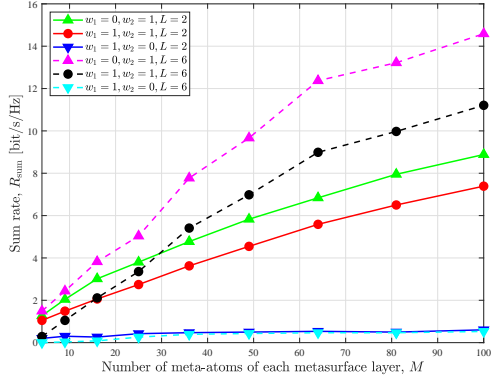


Fig. 3. Sum rate of communication users versus number of meta-atoms.

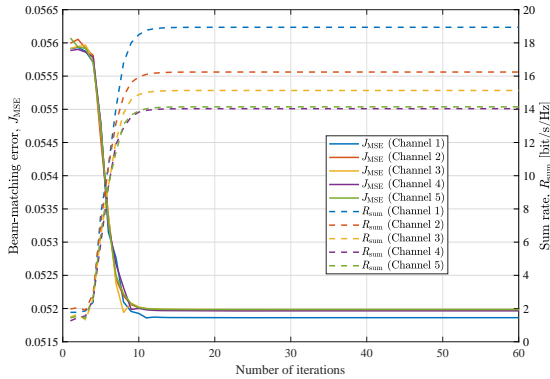


Fig. 4. Convergence analysis of the proposed D^3 algorithm ($M = 100$, $L = 10$, $w_1 = w_2 = 1$).

maintaining satisfactory sensing performance. This illustrates that our suggested D^3 method grants the SIM-enabled ISAC system to achieve both high-performance communication and sensing capabilities concurrently. Furthermore, Fig. 3 shows that the sum rate of users increases with the number of meta-atoms M and the number of layers L . This improvement is due to the additional flexibility in shaping the electromagnetic wavefront provided by the multi-layer massive metasurface array, which can enable more sophisticated beamforming patterns to better accommodate the dual-functional requirements.

Figure 4 depicts the convergence of the proposed D^3 algorithm. The solid lines represent beam-matching error (J_{MSE} , left y-axis), while the dashed lines show the sum rate of users (R_{sum} , right y-axis) over 60 iterations. Each color corresponds to a different channel realization. Notably, the D^3 algorithm converges rapidly in all cases, achieving its optimal value after approximately 15 iterations. This demonstrates that the proposed algorithm possesses the capacity to effectively adapt to different channel conditions, hence confirming its efficacy and reliability in practical ISAC systems.

V. CONCLUSION

This paper proposed a novel beamforming design for ISAC applications under the framework of transmit SIM-based antenna array. To realize a desirable dual-function performance trade-off, a non-convex MOP was established by simultaneously maximizing the communication sum rate and optimally shaping the sensing beam pattern by adjusting the reflection coefficients of the meta-atoms. To solve this problem, the D^3

algorithm was proposed, which effectively balances the trade-off between communication and sensing objectives through gradient differences and dual normalization. Numerical results confirmed the superiority of our proposed ISAC beamforming design under various channel conditions.

REFERENCES

- [1] S. Lu, F. Liu, Y. Li, K. Zhang, H. Huang, J. Zou, X. Li, Y. Dong, F. Dong, J. Zhu *et al.*, “Integrated sensing and communications: Recent advances and ten open challenges,” *IEEE Internet Things J.*, vol. 11, no. 11, pp. 19094–19120, Jun. 2024.
- [2] T. Mao, J. Chen, Q. Wang, C. Han, Z. Wang, and G. K. Karagiannidis, “Waveform design for joint sensing and communications in millimeter-wave and low Terahertz bands,” *IEEE Trans. Commun.*, vol. 70, no. 10, pp. 7023–7039, Oct. 2022.
- [3] F. Zhang, T. Mao, R. Liu, Z. Han, S. Chen, and Z. Wang, “Cross-domain dual-functional OFDM waveform design for accurate sensing/positioning,” *IEEE J. Sel. Areas Commun.*, to appear, 2024.
- [4] Y. Gong, Y. Wei, Z. Feng, F. R. Yu, and Y. Zhang, “Resource allocation for integrated sensing and communication in digital twin enabled Internet of Vehicles,” *IEEE Trans. Veh. Technol.*, vol. 72, no. 4, pp. 4510–4524, Apr. 2023.
- [5] R. Liu, L. Zhang, T. Mao, K. Guan, and Y. Xu, “Integrated sensing and communication for 6G: Motivation, enablers and standardization,” in *Proc. IEEE Int. Conf. Commun. China Workshops*, 2023, pp. 1–6.
- [6] W. Shi, W. Xu, X. You, C. Zhao, and K. Wei, “Intelligent reflection enabling technologies for integrated and green Internet-of-Everything beyond 5G: Communication, sensing, and security,” *IEEE Wirel. Commun.*, vol. 30, no. 2, pp. 147–154, Apr. 2023.
- [7] X. Liu, T. Huang, N. Shlezinger, Y. Liu, J. Zhou, and Y. C. Eldar, “Joint transmit beamforming for multiuser MIMO communications and MIMO radar,” *IEEE Trans. Signal Process.*, vol. 68, pp. 3929–3944, Jun. 2020.
- [8] C. Qi, W. Ci, J. Zhang, and X. You, “Hybrid beamforming for millimeter wave MIMO integrated sensing and communications,” *IEEE Commun. Lett.*, vol. 26, no. 5, pp. 1136–1140, May. 2022.
- [9] F. Liu, C. Masouros, A. P. Petropulu, H. Griffiths, and L. Hanzo, “Joint radar and communication design: Applications, state-of-the-art, and the road ahead,” *IEEE Trans. Commun.*, vol. 68, no. 6, pp. 3834–3862, Jun. 2020.
- [10] W. Tang, J. Y. Dai, M. Z. Chen, K.-K. Wong, X. Li, X. Zhao, S. Jin, Q. Cheng, and T. J. Cui, “MIMO transmission through reconfigurable intelligent surface: System design, analysis, and implementation,” *IEEE J. Sel. Areas Commun.*, vol. 38, no. 11, pp. 2683–2699, Nov. 2020.
- [11] C. Ma, X. Yang, J. Wang, G. Yang, W. Zhang, and S. Ma, “Reconfigurable distributed antennas and reflecting surface: A new architecture for wireless communications,” *IEEE Trans. Commun.*, to appear, 2024.
- [12] S. Xu, Y. Du, J. Zhang, J. Liu, J. Wang, and J. Zhang, “Intelligent reflecting surface enabled integrated sensing, communication and computation,” *IEEE Trans. Wirel. Commun.*, vol. 23, no. 3, pp. 2212–2225, Mar. 2024.
- [13] J. An, M. Di Renzo, M. Debbah, and C. Yuen, “Stacked intelligent metasurfaces for multiuser beamforming in the wave domain,” in *Proc. IEEE Int. Conf. Commun.*, 2023, pp. 2834–2839.
- [14] N. U. Hassan, J. An, M. Di Renzo, M. Debbah, and C. Yuen, “Efficient beamforming and radiation pattern control using stacked intelligent metasurfaces,” *IEEE Open J. Commun. Soc.*, vol. 5, pp. 599–611, Jan. 2024.
- [15] Z. Wang, H. Liu, J. Zhang, R. Xiong, K. Wan, X. Qian, M. Di Renzo, and R. Qiu, “Multi-user ISAC through stacked intelligent metasurfaces: New algorithms and experiments,” *arXiv preprint arXiv:2405.01104*, 2024.
- [16] J. An, C. Xu, D. W. K. Ng, G. C. Alexandropoulos, C. Huang, C. Yuen, and L. Hanzo, “Stacked intelligent metasurfaces for efficient holographic MIMO communications in 6G,” *IEEE J. Sel. Areas Commun.*, vol. 41, no. 8, pp. 2380–2396, Aug. 2023.
- [17] X. Lin, Y. Rivenon, N. T. Yardimci, M. Veli, Y. Luo, M. Jarrahi, and A. Ozcan, “All-optical machine learning using diffractive deep neural networks,” *Science*, vol. 361, no. 6406, pp. 1004–1008, Jul. 2018.
- [18] K. Meng, Q. Wu, R. Schober, and W. Chen, “Intelligent reflecting surface enabled multi-target sensing,” *IEEE Trans. Commun.*, vol. 70, no. 12, pp. 8313–8330, Dec. 2022.
- [19] L. Jiang and H. Jafarkhani, “Multi-user analog beamforming in millimeter wave MIMO systems based on path angle information,” *IEEE Trans. Wirel. Commun.*, vol. 18, no. 1, pp. 608–619, Jan. 2019.
- [20] D. P. Kingma and J. Ba, “Adam: A method for stochastic optimization,” *arXiv preprint arXiv:1412.6980*, 2014.